



<i>Title:</i> NEON Algorithm Theoretical Basis Document (ATBD): Fraction of Photosynthetically Active Radiation		<i>Date:</i> 03/28/2022
<i>NEON Doc. #:</i> NEON.DOC.003840	<i>Author:</i> T. Goulden	<i>Revision:</i> B

NEON ALGORITHM THEORETICAL BASIS DOCUMENT (ATBD): FRACTION OF PHOSYNTHETICALLY ACTIVE RADIATION

PREPARED BY	ORGANIZATION	DATE
Tristan Goulden	AOP	05/29/2019

APPROVALS	ORGANIZATION	APPROVAL DATE
Kate Thibault	SCI	03/28/2022

RELEASED BY	ORGANIZATION	RELEASE DATE
Tanisha Waters	CM	03/28/2022

See configuration management system for approval history.

The National Ecological Observatory Network is a project solely funded by the National Science Foundation and managed under a cooperative agreement by Battelle. Any opinions, findings, and conclusions or recommendations expressed in this material are those of the author(s) and do not necessarily reflect the views of the National Science Foundation.



<i>Title:</i> NEON Algorithm Theoretical Basis Document (ATBD): Fraction of Photosynthetically Active Radiation		<i>Date:</i> 03/28/2022
<i>NEON Doc. #:</i> NEON.DOC.003840	<i>Author:</i> T. Goulden	<i>Revision:</i> B

Change Record

REVISION	DATE	ECO #	DESCRIPTION OF CHANGE
A	07/01/2019	ECO-06170	Initial Release
B	03/28/2022	ECO-06791	<ul style="list-style-type: none">• Minor formatting updates• Added word NEON to document title



Title: NEON Algorithm Theoretical Basis Document (ATBD): Fraction of Photosynthetically Active Radiation		Date: 03/28/2022
NEON Doc. #: NEON.DOC.003840	Author: T. Goulden	Revision: B

TABLE OF CONTENTS

1 DESCRIPTION..... 1

1.1 Purpose..... 1

1.2 Scope..... 1

2 RELATED DOCUMENTS, ACRONYMS AND VARIABLE NOMENCLATURE..... 2

2.1 Applicable Documents..... 2

2.2 Reference Documents..... 2

2.3 Acronyms..... 2

3 DATA PRODUCT DESCRIPTION 3

3.1 Variables Reported..... 3

3.2 Input Dependencies..... 3

3.3 Product Instances..... 3

3.4 Temporal Resolution and Extent..... 3

3.5 Spatial Resolution and Extent..... 4

4 SCIENTIFIC CONTEXT..... 4

4.1 Theory of Measurement..... 4

5 ALGORITHM IMPLEMENTATION..... 7

6 UNCERTAINTY..... 9

6.1 Analysis of Uncertainty..... 11

6.2 Reported Uncertainty..... 15

7 VALIDATION AND VERIFICATION..... 16

8 FUTURE PLANS AND MODIFICATIONS 17

9 BIBLIOGRAPHY..... 18

LIST OF TABLES AND FIGURES

Table 1. Data products generated by algorithms described within this ATBD..... 3

Figure 1. Values for fPAR given SAVI (top) and LAI (bottom). 5

Figure 2. Workflow for creating the fPAR product..... 8

Figure 3. Number of overlapping flightlines for the ORNL BRDF flight. 13



<i>Title:</i> NEON Algorithm Theoretical Basis Document (ATBD): Fraction of Photosynthetically Active Radiation		<i>Date:</i> 03/28/2022
<i>NEON Doc. #:</i> NEON.DOC.003840	<i>Author:</i> T. Goulden	<i>Revision:</i> B

Figure 4. Uncertainty rasters and histograms of residuals of fPAR at SJER (top), SOAP (middle), and ORNL (bottom). Red line on the histogram represents a normal distribution curve with the mean and standard deviation of the residuals.....14

Figure 5. Section of a single flight line showing, left: fPAR, center: uncertainty in fPAR, right: uncertainty as a percentage of fPAR.....15



<i>Title:</i> NEON Algorithm Theoretical Basis Document (ATBD): Fraction of Photosynthetically Active Radiation		<i>Date:</i> 03/28/2022
<i>NEON Doc. #:</i> NEON.DOC.003840	<i>Author:</i> T. Goulden	<i>Revision:</i> B

1 DESCRIPTION

1.1 Purpose

This document details the algorithms used for creating the NEON Level 2 **fPAR** data product (NEON.DOM.SITE.DP2.30014) from Level 1 data, and ancillary data (such as calibration data), obtained via instrumental measurements made by the Neon Imaging Spectrometer (NIS) sensor on Airborne Observation Platform (AOP). It includes a detailed discussion of measurement theory and implementation, appropriate theoretical background, data product provenance, quality assurance and control methods used approximations and/or assumptions made, and a detailed exposition of uncertainty resulting in a cumulative reported uncertainty for this product.

1.2 Scope

This document describes the theoretical background and entire algorithmic process for creating NEON.DOM.SITE.DP2.30014 from input data. It does not provide computational implementation details, except for cases where these stem directly from algorithmic choices explained here.



Title: NEON Algorithm Theoretical Basis Document (ATBD): Fraction of Photosynthetically Active Radiation		Date: 03/28/2022
NEON Doc. #: NEON.DOC.003840	Author: T. Goulden	Revision: B

2 RELATED DOCUMENTS, ACRONYMS AND VARIABLE NOMENCLATURE

2.1 Applicable Documents

AD[01]	NEON.DOC.000001	NEON Observatory Design (NOD) Requirements
AD[02]	NEON.DOC.002652	NEON Level 1, Level 2 and Level 3 Data Products Catalog
AD[03]	NEON.DOC.001984	AOP flight plan boundaries design
AD[04]	NEON.DOC.002890	NEON AOP Level 0 quality checks
AD[05]	NEON.DOC.001207	NEON imaging spectrometer geolocation algorithm theoretical basis document
AD[06]	NEON.DOC.002649	NEON configured site list

2.2 Reference Documents

RD[01]	NEON.DOC.000008	NEON Acronym List
RD[02]	NEON.DOC.000243	NEON Glossary of Terms
RD[03]	NEON.DOC.005011	NEON Coordinate Systems Specification
RD[04]	NEON.DOC.002890	NEON AOP Level 0 quality checks
RD[05]	NEON.DOC.001984	AOP flight plan boundaries design
RD[06]	NEON.DOC.001292	NEON Imaging Spectrometer Geolocation Algorithm Theoretical Basis Document
RD[07]	NEON.DOC.001288	NEON Imaging Spectrometer Radiance to Reflectance Algorithm Theoretical Basis Document
RD[08]	NEON.DOC.002391	NEON Normalized Difference Vegetation Index (NDVI), Enhanced Vegetation Index (EVI), Atmospherically Resistant Vegetation Index (ARVI), Canopy Xanthophyll Cycle (PRI), and Canopy Lignin (NDLI) Algorithm Theoretical Basis Document
RD[09]	NEON.DOC.002385	NEON Leaf Area Index (LAI) Algorithm Theoretical Basis Document

2.3 Acronyms

Acronym	Explanation
NIS	NEON Imaging Spectrometer
ITRF00	International Terrestrial Reference Frame 2000
UTM	Universal Transverse Mercator
TIFF	Tagged Image File Format
AOP	Airborne Observation Platform
FBO	Fixed Base Operator
SAVI	Soil Adjusted Vegetation Index
LAI	Leaf Area Index
VI	Vegetation index
fPAR	Fraction of Photosynthetically Active Radiation



Title: NEON Algorithm Theoretical Basis Document (ATBD): Fraction of Photosynthetically Active Radiation		Date: 03/28/2022
NEON Doc. #: NEON.DOC.003840	Author: T. Goulden	Revision: B

3 DATA PRODUCT DESCRIPTION

3.1 Variables Reported

The products supplied through NEON.DOM.SIT.DP2.30014 include an fPAR (fraction of photosynthetically active radiation) map and fPAR uncertainty map, both in raster format by flight line. The fPAR and fPAR uncertainty maps are derived from the directional surface reflectance RD[07], through the intermediate SAVI (Soil Adjusted Vegetation Index) and LAI (Leaf Area Index) products. Raster maps for fPAR and fPAR uncertainty are reported with horizontal reference to the ITRF00 datum, projected to the Universal Transverse Mercator (UTM) mapping frame in accordance with RD[03]. The fPAR is reported as a unit-less value which describes the fraction of absorbed vs incident solar radiation by plant material. The product is stored in a GeoTIFF format in accordance with the GeoTIFF specification (Ritter et al., 2000).

3.2 Input Dependencies

The creation of fPAR rasters is dependent on the creation of the bi-directional surface reflectance, and is based on the SAVI and LAI products. Procedures for creating SAVI can be found in RD[08] and for LAI in RD[09].

3.3 Product Instances

The NEON data products produced directly from these algorithms are summarized in **Table 1**.

Table 1. Data products generated by algorithms described within this ATBD.

Data product identification	Data product name
NEON.DOM.SITE.DP2.30014	fPAR

3.4 Temporal Resolution and Extent

The fPAR products are derived from data collected during acquisition of a single core, re-locatable or aquatic site by the AOP (Airborne Observation Platform). Depending on external variables such as weather, transit time to the site FBO (Fixed Based Operator), and total area of the priority 1 flight box (see RD[05]), the temporal resolution of a single acquisition of LO NIS information could range from a single flight (4 hrs) to several flights acquired over multiple days. Generally, due to the peak greenness constraint of AOP data acquisition (site at > 90% peak greenness value), and the requirement that all sites are to be flown annually, the total potential time to acquire a site will have a limit which defines the largest temporal resolution for a single acquisition. Details defining the total amount of potential time dedicated to a single site acquisition are given in RD[05]. As the NEON AOP payload is scheduled to repeat each NEON site on an annual basis, the temporal resolution of multiple acquisitions will be one year.



Title: NEON Algorithm Theoretical Basis Document (ATBD): Fraction of Photosynthetically Active Radiation		Date: 03/28/2022
NEON Doc. #: NEON.DOC.003840	Author: T. Goulden	Revision: B

3.5 Spatial Resolution and Extent

The spatial resolution and extent of the fPAR product will be equivalent to the spatial resolution and extent of the surface directional reflectance. The fPAR product relies on the intermediate calculation of SAVI (RD[08]) and LAI (RD[09]), which both shall maintain 1 m spatial resolution. The spatial extent of the fPAR maps will relate to the definition of the AOP flight box for each individual site (RD[04]). It is intended that a minimum of 80% of the priority 1 flight box and 95% of the tower airshed will be acquired each year (RD[07]). As discussed in Section 3.4, the actual acquired area could vary depending on external conditions encountered during the flight. Ultimately, the flight schedule as defined in RD[04] shall supersede the percent coverage requirement. Therefore, the actual acquired spatial extent may vary annually.

4 SCIENTIFIC CONTEXT

The fraction of photosynthetically active radiation describes the relative quantity of incident solar radiation of relevant photosynthetically active wavelengths (0.4-0.7 μm) absorbed by vegetative material. Photosynthetic capacity photosynthetically drives the exchange of gases and water vapor within plant material, therefore fPAR is an important data source for simulation of water, carbon and nutrient cycling (Sellers et al., 1997; Jarvis, 1976). Due to this role, fPAR is an important physical component in temporal assessments of changes to vegetative productivity and health, and as an input data layer for simulation models that allow prediction of ecological response to climate volatility. An applied example of such a model is the SiB2 general circulation model (GCM) developed by Sellers et al. (1996). The SiB2 utilizes remote-sensing derived fPAR as an input parameter to the embedded integrated canopy photosynthesis-conductance model (see Sellers (1985)) which can be used to inform photosynthetic rates and evapotranspiration (ET) over large spatial scales (Sellers et al., 1996).

4.1 Theory of Measurement

The calculation of fPAR implements the methodology reported by Richter and Schläpfer (2014). Following the theoretical justification in Section 4.1, the calculation of fPAR is related to the measured surface reflectance through the calculation of SAVI and LAI. The SAVI is determined through the following equation (Huete, 1988):

$$SAVI = \frac{(\rho_{NIR} - \rho_R)(1 + L)}{(\rho_{NIR} - \rho_R + L)}$$

where L is a user-defined adjustment parameter set to 0.5. Following SAVI, the LAI is calculated with the following equation

$$LAI = -\frac{1}{a_2} \ln\left(\frac{a_2 - SAVI}{a_1}\right)$$



Title: NEON Algorithm Theoretical Basis Document (ATBD): Fraction of Photosynthetically Active Radiation		Date: 03/28/2022
NEON Doc. #: NEON.DOC.003840	Author: T. Goulden	Revision: B

where a_0 , a_1 , a_2 are user defined parameters set to 0.82, 0.78, and 0.6 respectively. For details on the algorithmic choices made for calculation of LAI, the reader is referred to RD[09]. Following LAI, fPAR can be calculated with a three parameter model as described in Richter and Schläpfer (2014) and originally formulated in Asrar et al. (1984)

$$fPAR = C[1 - A \exp(-B \cdot LAI)]$$

where A , B , and C are parameters which are currently set to 1, 0.4, and 1 respectively. During future analysis these parameters may be modified to adapt to the unique conditions at specific NEON sites (see Section 6).

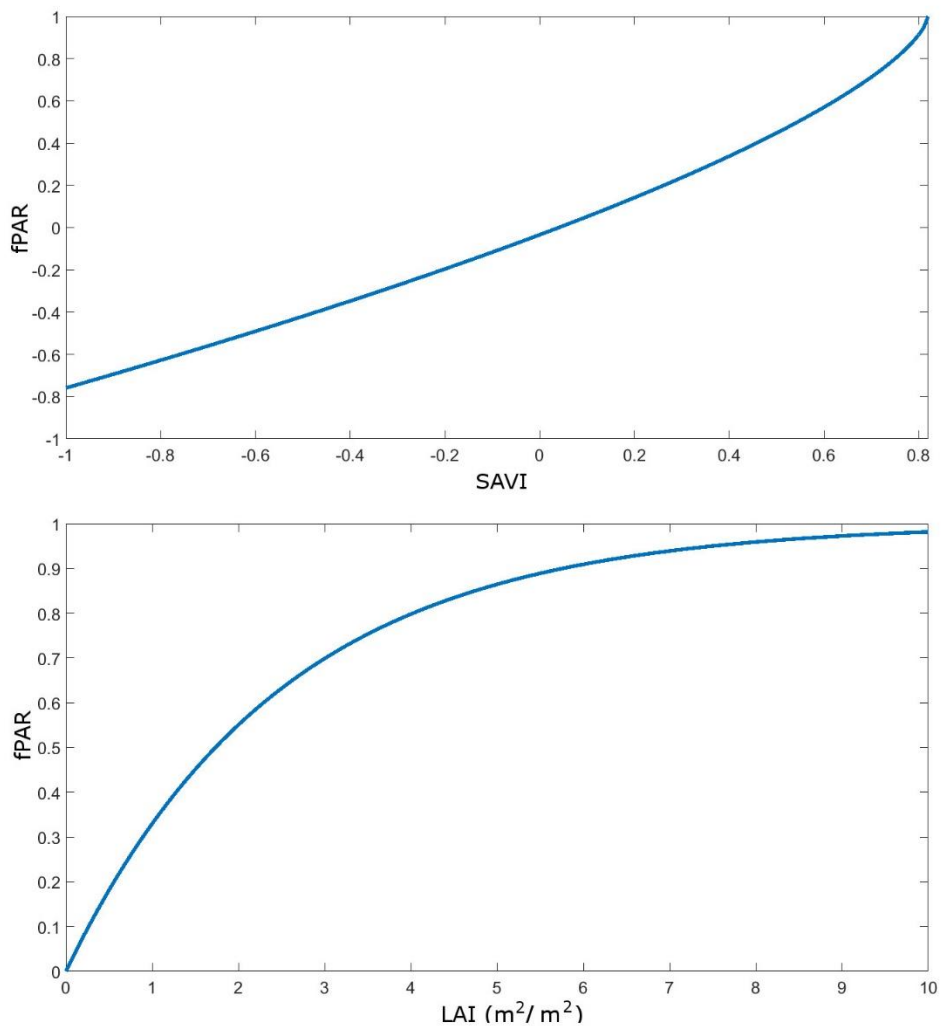


Figure 1. Values for fPAR given SAVI (top) and LAI (bottom).



Title: NEON Algorithm Theoretical Basis Document (ATBD): Fraction of Photosynthetically Active Radiation		Date: 03/28/2022
NEON Doc. #: NEON.DOC.003840	Author: T. Goulden	Revision: B

During the calculation of fPAR, the location of the ρ_{NIR} and ρ_R bands must be selected from the available 5 nm bands recorded by the NIS. Richter and Schläpfer (2014) suggest that the wavelength regions around 850 nm and 650 nm for ρ_{NIR} and ρ_R respectively for use in calculating SAVI. Within each NIS, it is unlikely a band will be centered exactly on 850 nm or 650 nm, and an appropriate spectral bandpass containing the relevant data must be selected. A straightforward solution selects the bands whose centers closely match 850 nm and 650 nm, however this under utilizes a vast amount of information collected by the NIS in the surrounding bands. Additionally, the central wavelength of the nearest band may be varied across instruments, resulting in small inconsistencies in products derived from each NIS. A solution is to retrieve regions of ρ_{NIR} and ρ_R which are wider than 5 nm but centered on the desired wavelength.

To appropriately sample a wider spectral region, a Gaussian averaging routine is implemented. The Gaussian averaging algorithm associates weights with each spectral band surrounding the central location of ρ_{NIR} and ρ_R . The weights are determined according to a Gaussian function which gives the highest weights to bands near the center of the Gaussian curve and that decrease further from the center. The definition of the Gaussian curve requires two parameters, the center and the standard deviation (σ). The center is chosen to correspond to ideal wavelengths (850 nm and 650 nm for ρ_{NIR} and ρ_R respectively), while σ controls the weights. A higher σ results in a wider Gaussian curve with less decay on the weights with further distance from the central wavelength while a smaller value of σ results in a Gaussian curve with rapid decay which primarily uses the information in the immediate region around the center wavelength. The Gaussian curve takes the following well-known formula

$$f(x) = e^{-(x-\rho)^2/2\sigma^2}$$

where ρ represents the central wavelength. Values for the Gaussian weights (GW) can be obtained by substituting the difference for each band center and the central location of either ρ_{NIR} and ρ_R into Equation (4). Theoretically, the Gaussian curve extends to infinity, but drops quickly from its peak at ρ . Therefore, as a practical limitation, only bands within two σ (95%) of the Gaussian curve are included in the derivation of GW . The weighted Gaussian average is determined by the sum, of an element-wise multiplication (denoted by \odot) of GW by the associated reflectance values (R), and division by the sum of the weights:

$$GA = \frac{\sum[R \odot GW]}{\sum GW}$$

The calculations for fPAR then proceed by applying Equation (5) to the spectral regions surrounding ρ_{NIR} and ρ_R and substituting into Equation (1), through Equation (3).



Title: NEON Algorithm Theoretical Basis Document (ATBD): Fraction of Photosynthetically Active Radiation		Date: 03/28/2022
NEON Doc. #: NEON.DOC.003840	Author: T. Goulden	Revision: B

5 ALGORITHM IMPLEMENTATION

The processing of surface reflectance into the fPAR product is achieved through the steps outlined in this section (**Figure 2**). The algorithm for fPAR is implemented through multiple interconnected Matlab functions which automate the algorithm. The process is dependent on only the existence of surface reflectance and several input parameters listed below. Details into the algorithm which creates the input surface reflectance can be found in RD[07].

Step 1:

Calculate Gaussian average of desired bands to determine ρ_R and ρ_{NIR} according to Equation (5).

Input:

1. reflectance data (HDF5 format)
2. band center for ρ_R
3. band center for ρ_{NIR}
4. sigma (σ) for defining width of Gaussian weighting curve

Output: Gaussian weighted bands for ρ_R and ρ_{NIR}

Functions used: calc_Gaussian_average.m

Step 2:

Calculate SAVI raster according to Equation (1) using output from Step 1.

Input:

1. ρ_R and ρ_{NIR} from Step 1
2. SAVI user defined constant (L), described in Equation (1)

Output: SAVI in geotiff format

Functions used: calc_SAVI.m

Step 3:

Calculate LAI raster according to Equation (2) using output from Step 2.

Input:

1. SAVI raster from Step 2
2. User defined parameters described in Equation (2), including a_0, a_1, a_2 .

Output: LAI raster in Geotiff format

Functions used: calc_LAI.m

Step 4:

Calculate fPAR raster according to Equation (3) using output from Step 3.

Input:

1. LAI raster from Step 3
2. User defined parameters described in Equation (3), including A, B, C.



Output: LAI raster in Geotiff format

Functions used: calc_fPAR_v01.m

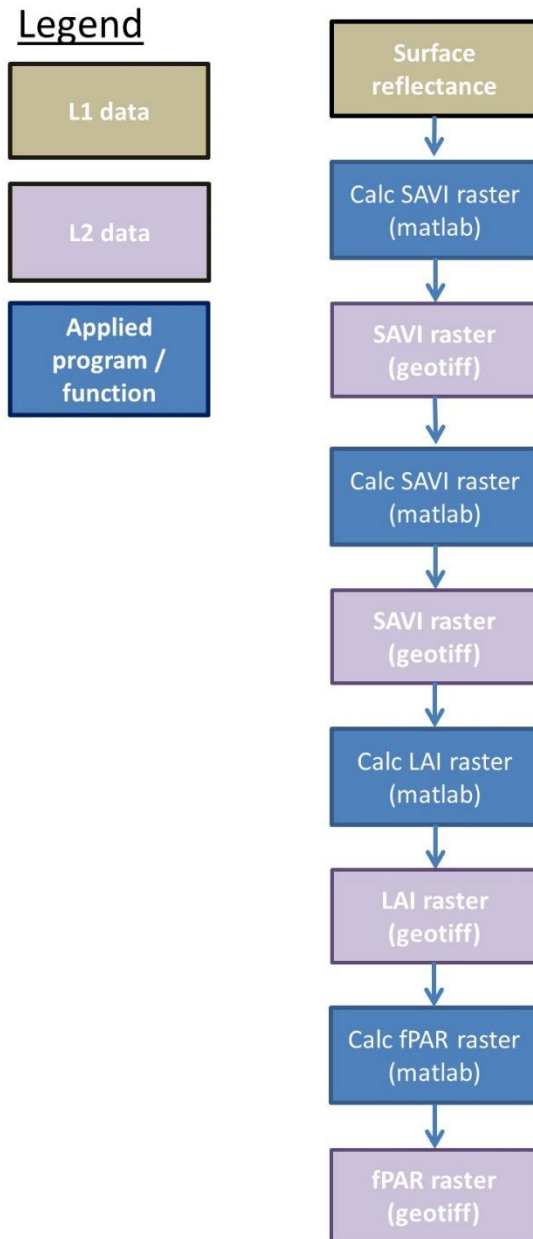


Figure 2. Workflow for creating the fPAR product.



Title: NEON Algorithm Theoretical Basis Document (ATBD): Fraction of Photosynthetically Active Radiation		Date: 03/28/2022
NEON Doc. #: NEON.DOC.003840	Author: T. Goulden	Revision: B

6 UNCERTAINTY

The uncertainty in fPAR is derived from the uncertainty in the surface reflectance product. Richter and Schläpfer (2014) and Richter and Schläpfer (2002) indicate that ATCOR is capable of providing retrieved surface reflectance values of $\pm 2\%$ when the reflectance value is $< 10\%$, and $\pm 4\%$ when reflectance is $> 40\%$. However, these values are only achievable if the uncertainty in several additional sources is controlled including:

1. calibration of the sensor
2. quality of geometric co-registration of the spectral bands
3. quality of the ortho-rectification
4. accuracy of the radiative transfer code (MODTRAN 5)
5. correct choice of the atmospheric input parameters
6. terrain type (flat vs. rugged)
7. surface cover

NEON undertakes annual calibrations of the imaging spectrometer, which will minimize errors due to source 1. Currently, the uncertainty introduced through calibration is not strictly quantified and propagated into derived products. Vicarious calibration surveys are performed over homogeneous targets (concrete, consistent low vegetation) at the beginning and end of the annual flight campaign, including ground validation of targets with known reflectance measured with a field spectrometer. This information allows an annual empirical assessment of the calibration uncertainty which is used to verify the quality of the calibration. Additional research will be necessary to propagate the calibration uncertainty through to final products. Results of the annual vicarious calibration tests indicate that the error is small ($< 0.5\%$), indicating its effect may be negligible.

Internal testing has shown sub-pixel accuracy of the ortho-rectification (source 3), which is based on a spectrometer camera model described in RD[06]. The individual spectral bands are collected simultaneously on a single focal plane array, introducing negligible error in co-registration between spectral bands (source 2). Therefore, it can be assumed that the geo-location error does not introduce a significant level of uncertainty into resulting surface reflectance in flat or smoothly undulating terrain. However, as identified in Richter and Schläpfer (2014), highly rugged terrain such as mountainous environments can introduce a mis-registration between the DSM and reflectance measurements which can cause errors in surface reflectance greater than $\pm 100\%$ (due to error source 6). Richter and Schläpfer (2014) recommend that the DSM spatial resolution is one-third or one-quarter the spatial resolution of the imaging spectrometer data. However the DSMs at NEON are created at equivalent resolutions (1 m) due to limitations in the point density of the LiDAR system. At current nominal altitudes and LiDAR system collection parameters, the resulting point spacing is not capable of confidently supporting DSM grid resolutions below 1 m spatial resolution. Therefore, user's should be aware that data located near sharp peaks or ridges should be



Title: NEON Algorithm Theoretical Basis Document (ATBD): Fraction of Photosynthetically Active Radiation		Date: 03/28/2022
NEON Doc. #: NEON.DOC.003840	Author: T. Goulden	Revision: B

treated with extreme caution as the uncertainty may be extremely high. NEON data does maintain an advantage in reducing uncertainty due to terrain effects by simultaneously collecting the NIS and LiDAR from co-mounted sensors on the same platform, and creating the spectrometer camera model using intensity images from the LiDAR. This provides a high level of relative accuracy between the DSM and spectrometer, minimizing uncertainty due to the terrain conditions. Typically, geo-location errors are highest at strip edges due to limitations in derivation of the geo-location model (see RD[06]). Therefore, the combination of mountainous terrain and data acquired at strip edges will introduce the largest sources of uncertainty in geo-location.

The retrieval of surface reflectance is performed with ATCOR, which is a commercial off-the-shelf software package (see RD[07]), preventing NEON from controlling the uncertainty introduced through source 4, the accuracy of radiative transfer code derived from MODTRAN 5. It is assumed that this is being correctly implemented within ATCOR, and that efforts to minimize the uncertainty due to this source were applied. User's should be aware that ATCOR does not explicitly calculate a radiative transfer model for every observation. For processing efficiency, ATCOR pre-generates a series of look-up tables which are representative of common atmospheric and flight conditions (altitude, aerosol loading, visibility humidity etc.). Some uncertainty will be introduced through interpolation of true conditions to the most representative scenarios in the look up tables (LUTs). Assuming error source 4 is well-controlled within ATCOR and appropriate conditions are available in the LUTs, the primary source of error affected by NEON processing procedures is due to source 5, the correct choice of atmospheric input parameters. Currently, a standard set of parameters is selected across all NEON sites, and no attempt is made to dynamically vary the input parameters for unique site conditions. Details into the implemented input parameters can be found in RD[07]. As the NEON project continues, research will be undertaken to allow the conditions experienced during flight to inform the correct selection of parameters for atmospheric correction, and better quantify the uncertainty introduced in these choices.

In addition to the uncertainty introduced by ATCOR, there is an inherent uncertainty related to the empirical equation used to calculate fPAR (Equation (3)), and the values selected of the parameters (A, B, C). The original relationship and parameters are optimized for a particular sensor, vegetation type, and phenological stage and age of the observed vegetation. As modeled relationship and parameterizations of physical quantities from VIs can be specific to space, time and species (Houborg, Soegaard, & Boegh, 2007; Ganguly et al., 2014), this method is not ideally suited for calculating fPAR across the diversity of NEON sites and through the lifetime of the observatory. For example, Colombo, Bellingeri, Fasolini, and Marino (2003) summarizes the confounding factors which can affect modeled relationships / parameters between LAI and VI to include 1) vegetation type, 2) background reflectance, 3) crown closure and leaf orientation of leaf elements, 4) influence from branches, 5) stand age, and 6) chlorophyll concentration. Richter and Schläpfer (2014) identify that the implementation of static parameters may lead to a loss in absolute accuracy, however the relative accuracy between collections at distinct instances in time will be acceptable. This is beneficial to user's of NEON data analyzing annual vegetative change, potentially



Title: NEON Algorithm Theoretical Basis Document (ATBD): Fraction of Photosynthetically Active Radiation		Date: 03/28/2022
NEON Doc. #: NEON.DOC.003840	Author: T. Goulden	Revision: B

allowing these applications to be proceed. NEON attempts to reduce the uncertainty introduced through annual observations by collecting during periods of at least 90% peak greenness. However, studies such as Colombo et al. (2003) suggest that empirical relationships with static parameters are not necessarily valid through time given the changes in the vegetation life-cycle, implying relative changes be invalid even if the data are captured at the same occurrence in the phenological cycle. This is not surprising as statistical derived empirical relationship do not model the true general physical relationship between physical properties and vegetative photosynthetic capacity as represented by observed reflectance spectra (Wang et al., 2004). Given few studies have analyzed quantification of fPAR at the spatial resolution observed by NEON, with the same diversity of sites, and with a comparable sensor future research will have to inform more sophisticated algorithms for accurate quantification of fPAR with appropriate quantification of uncertainty associated with algorithmic choices. Currently, sufficient ground data it is unavailable to test the error in absolute measurements of fPAR, therefore user’s should consider these implications when drawing conclusions derived from NEON-derived fPAR. Especially if implementing NEON derived fPAR into data layers for simulating and extrapolating environmental phenomena to large scales.

6.1 Analysis of Uncertainty

Given an absolute assessment of the uncertainty in fPAR is not possible, the analysis of uncertainty in the fPAR product is conducted through two methods which provide estimates on the repeatability (precision) of the product: 1) theoretical error propagation techniques using assumptions about the nature of uncertainty in the derived reflectance and 2) empirical assessments using data acquired from flights with multiple overlapping strips. For **method 1** it is assumed that the uncertainty in reflectance is approximately 5%, closely following the suggestion of Richter and Schläpfer (2014). Rasters of simulated uncertainty in fPAR are calculated by propagating the 5% uncertainty through Equation (3). The error propagation is conducted through the GLOPOV (General Law of Propagation of Variances). The GLOPOV states that the sum of squares of the function’s partial derivatives of each observable quantity, multiplied by the variance in the observable quantity will provide the total propagated error if the observations are statistically independent (Wolf & Ghilani, 2006) as follows:

$$\sigma_{fPAR}^2 = \left[\frac{\delta fPAR}{\delta \rho_R} \right] \sigma_{\rho_R}^2 + \left[\frac{\delta fPAR}{\delta \rho_{NIR}} \right] \sigma_{\rho_{NIR}}^2$$

where σ_{ρ_R} and $\sigma_{\rho_{NIR}}$ are the uncertainties in the reflectance values for the R and NIR bands respectively. Both σ_{ρ_R} and $\sigma_{\rho_{NIR}}$ are assumed to be statistically independent. The independence assumption between the bands typically leads to an over estimation in the propagated uncertainty in fPAR. However, it should be noted that assuming statistical independence between bands ignores any auto-correlation in error between spectral bands and indicates spectral averaging through Equation (5) will reduce the uncertainty through averaging. Preliminary observation / assessment of errors in reflectance show that the random



Title: NEON Algorithm Theoretical Basis Document (ATBD): Fraction of Photosynthetically Active Radiation		Date: 03/28/2022
NEON Doc. #: NEON.DOC.003840	Author: T. Goulden	Revision: B

component is minor, while constant (or highly correlated) random bias appears to dominate. Therefore, no reduction in error is applied in the process of Gaussian Averaging to maintain a conservative estimate of the error.

Method 2 of uncertainty assessment leverages flights undertaken to assess the BRDF (bi-directional reflectance distribution function) of the spectrometer in different eco-systems. The BRDF flights are designed as a series of over-lapping lines from multiple different directions resulting in a 'star' pattern with several flightlines overlapping near the center (**Figure 3**). Multiple over-lapping fPAR products were created, one for each flightline. Since each line is spatially referenced to the same 1 m UTM grid, the standard deviation of pixels at the same location, but sampled from multiple flight lines can be used as a proxy for the uncertainty in terms of repeatability at each pixel. A rectangular box which contains the area where the majority of lines overlapped was extracted and used for analysis (**Figure 3**). A generalized site wide estimate of uncertainty is derived from the standard deviation of all residuals (difference of the value at a pixel and the mean of the pixel) across the entire analyzed area. At the time of writing, BRDF flights have been acquired at ORNL (Oak Ridge National Laboratory), SOAP (Soaproot Saddle), and SJER (San Joaquin Experimental Range) which represent three end member ecosystems including close canopy Oak and Hickory forest, open canopy composed of Ponderosa Pines, and open Savannah dominated by Blue Oak, respectively. The results of the empirical analysis on the BRDF flights showed that the site-wide repeatability of fPAR (standard deviation of residuals) at standard confidence was approximately ± 0.08 (0.16 @ 95%), ± 0.08 (0.16 @ 95%), ± 0.04 (0.08 @ 95%) at ORNL, SOAP and SJER respectively. The rasters of uncertainty exhibited spatial patterns related to landscape characteristics, which cause the deviation of residuals from normal distributions (**Figure 4**). Currently investigations are on-going to better quantify the landscape factors which drive the uncertainty in fPAR. Users should be aware that this level of error may exist in any given pixel of the fPAR product.

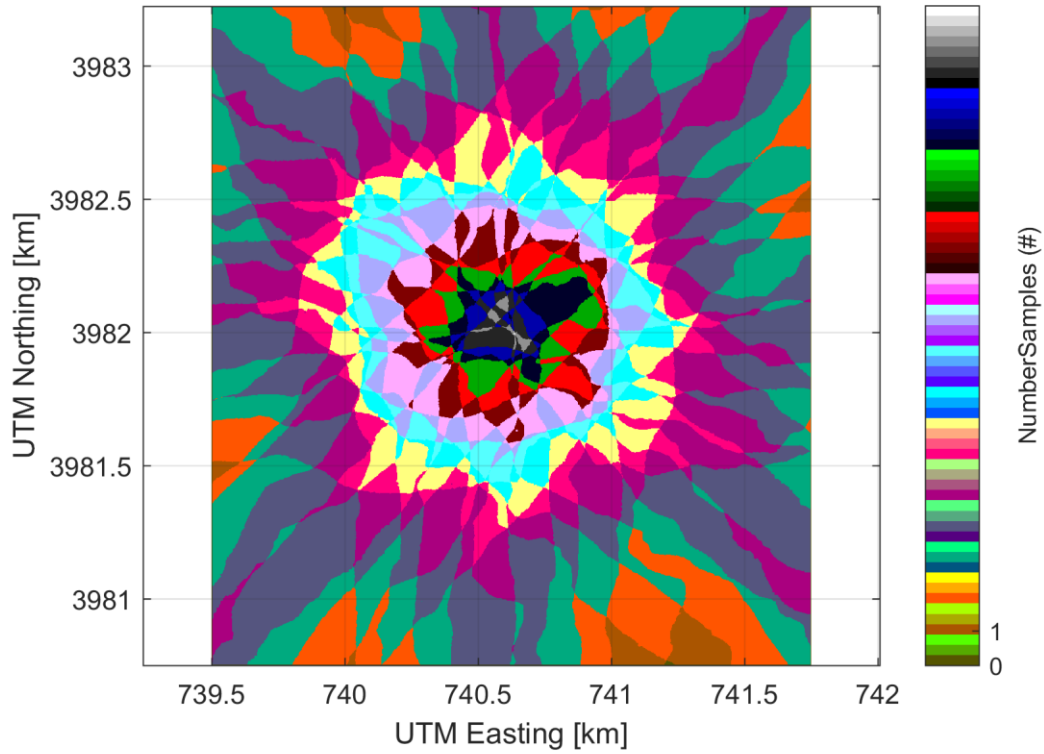


Figure 3. Number of overlapping flightlines for the ORNL BRDF flight.

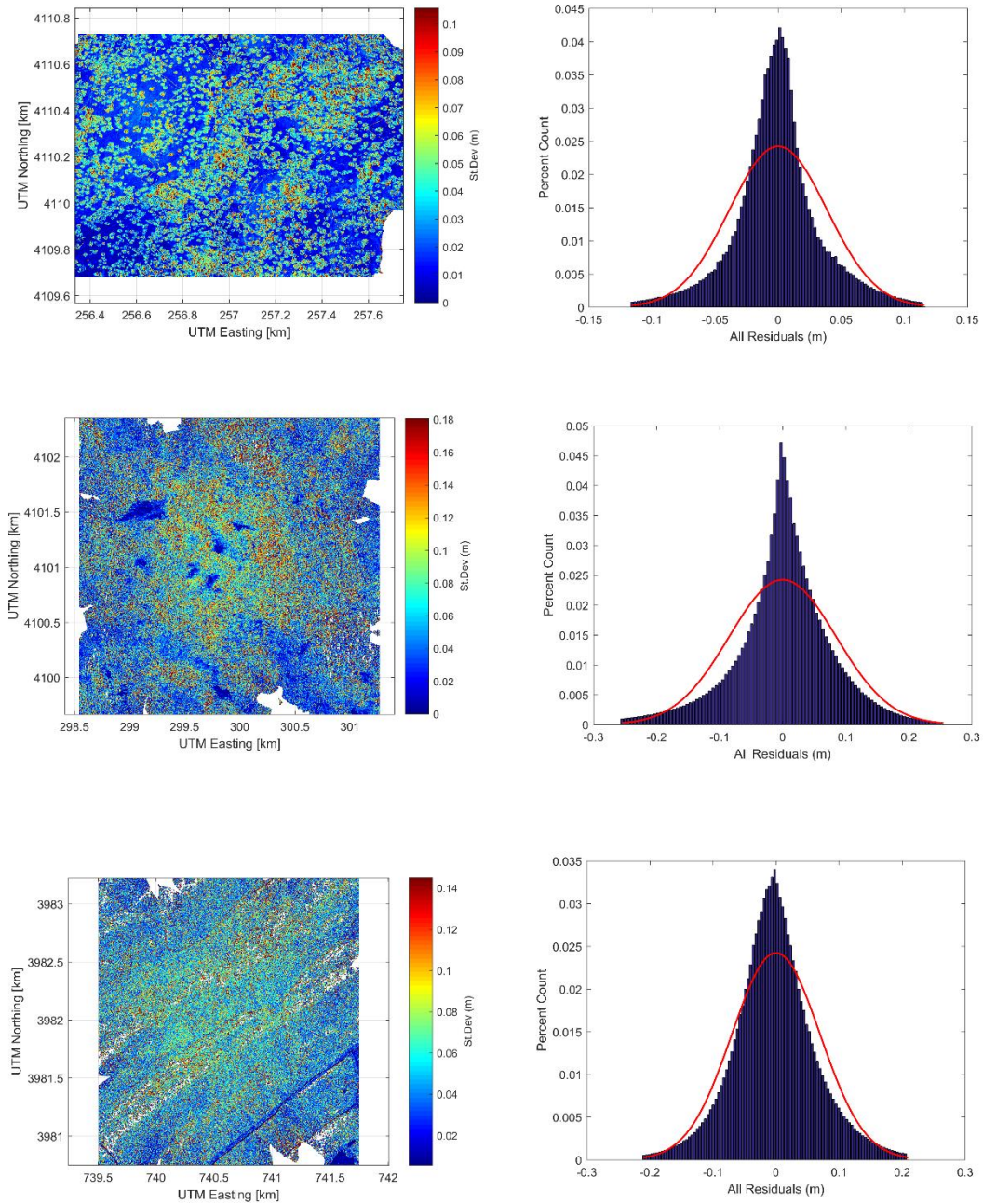


Figure 4. Uncertainty rasters and histograms of residuals of fPAR at SJER (top), SOAP (middle), and ORNL (bottom). Red line on the histogram represents a normal distribution curve with the mean and standard deviation of the residuals.



6.2 Reported Uncertainty

The uncertainty is reported as an uncertainty raster with the same dimensions and spatial resolution as the original flight line (**Figure 5**). Each pixel is calculated according to Equation (6) and provided as a Geotiff with the Geotiff of fPAR.

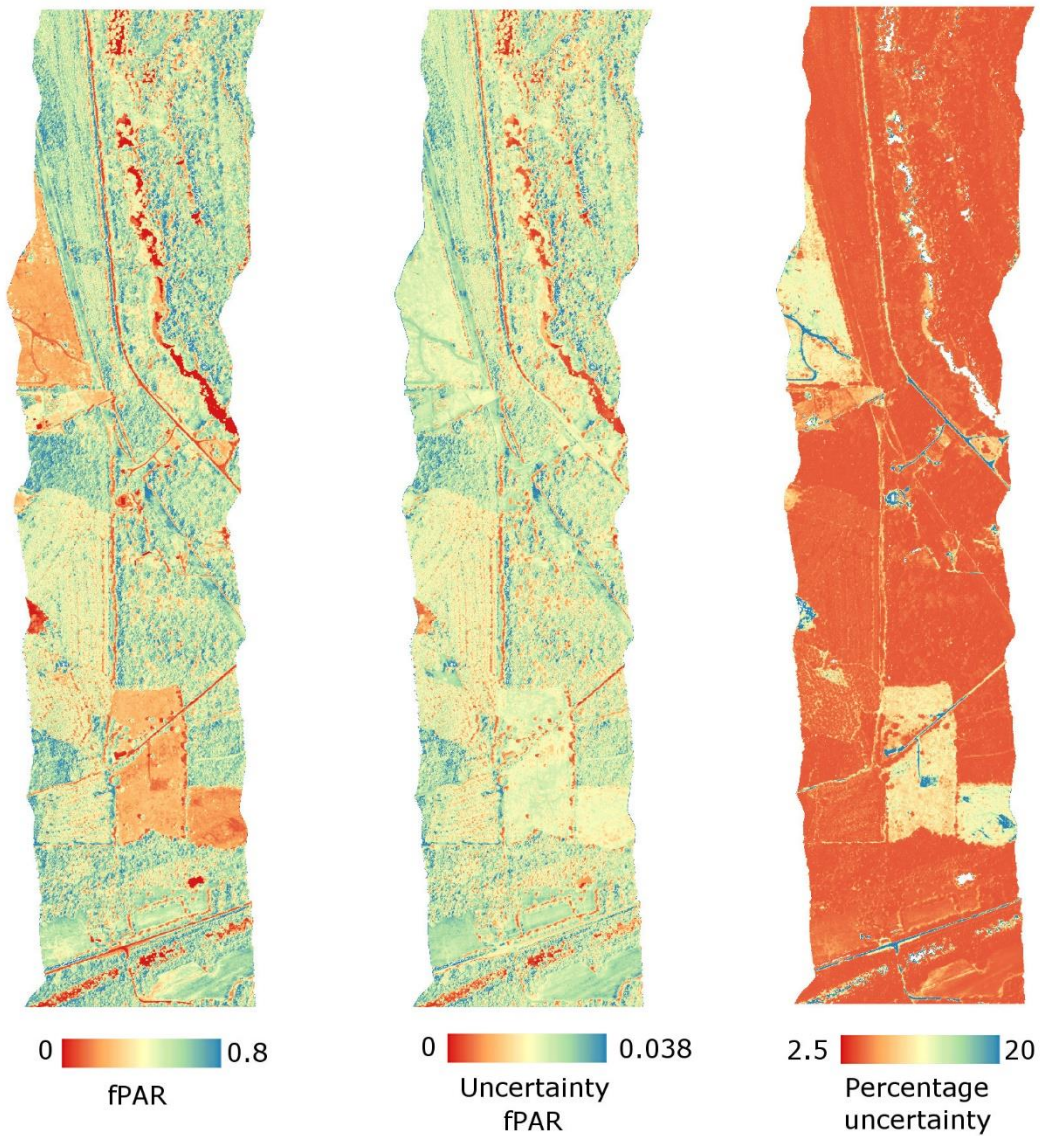


Figure 5. Section of a single flight line showing, left: fPAR, center: uncertainty in fPAR, right: uncertainty as a percentage of fPAR.



<i>Title:</i> NEON Algorithm Theoretical Basis Document (ATBD): Fraction of Photosynthetically Active Radiation		<i>Date:</i> 03/28/2022
<i>NEON Doc. #:</i> NEON.DOC.003840	<i>Author:</i> T. Goulden	<i>Revision:</i> B

7 VALIDATION AND VERIFICATION

The fPAR product was validated through comparison with the output from ATCOR, which the product was modeled after. Differences when compared to the ATCOR output were minor and assumed to be a result of the Gaussian weight-ing algorithm. The close agreement between the outputs and ATCOR indicated there were no fundamental flaws in the algorithm.



<i>Title:</i> NEON Algorithm Theoretical Basis Document (ATBD): Fraction of Photosynthetically Active Radiation		<i>Date:</i> 03/28/2022
<i>NEON Doc. #:</i> NEON.DOC.003840	<i>Author:</i> T. Goulden	<i>Revision:</i> B

8 FUTURE PLANS AND MODIFICATIONS

Currently, the primary upgrades planned for the fPAR product are related to development of a more sophisticated algorithm. Ideally, the algorithm will take the form of a physically based theoretical derivation which will allow general relationships to be appropriately applied to all sites within the NEON project, or to determine unique regionally based models through statistical or machine learning approaches. Each choice will require sufficient ground truth data to appropriately validate and calibrate model outputs, which will be the primary limiting factor for future model development.



Title: NEON Algorithm Theoretical Basis Document (ATBD): Fraction of Photosynthetically Active Radiation		Date: 03/28/2022
NEON Doc. #: NEON.DOC.003840	Author: T. Goulden	Revision: B

9 BIBLIOGRAPHY

- Asrar, G., Fuchs, M., Kanemasu, E., & Hatfield, J. (1984). Estimating absorbed photosynthetic radiation and leaf area index from spectral reflectance in wheat. *Agronomy journal*, 76(2), 300–306.
- Colombo, R., Bellingeri, D., Fasolini, D., & Marino, C. M. (2003). Retrieval of leaf area index in different vegetation types using high resolution satellite data. *Remote Sensing of environment*, 86(1), 120–131.
- Ganguly, S., Nemani, R. R., Baret, F., Bi, J., Weiss, M., Zhang, G., ..., Verger, A., et al. (2014). Green leaf area and fraction of photosynthetically active radiation absorbed by vegetation. In *Biophysical applications of satellite remote sensing* (pp. 43–61). Springer.
- Hatfield, J., Asrar, G., & Kanemasu, E. (1984). Intercepted photosynthetically active radiation estimated by spectral reflectance. *Remote Sensing of Environment*, 14(1-3), 65–75.
- Houborg, R., Soegaard, H., & Boegh, E. (2007). Combining vegetation index and model inversion methods for the extraction of key vegetation biophysical parameters using terra and aqua modis reflectance data. *Remote Sensing of Environment*, 106(1), 39–58.
- Huete, A. (1988). A soil-adjusted vegetation index. *Remote Sensing Of Environment*.
- Jarvis, P. (1976). The interpretation of the variations in leaf water potential and stomatal conductance found in canopies in the field. *Philosophical Transactions of the Royal Society of London. Series B, Biological Sciences*, 593–610.
- Myneni, R. & Williams, D. (1994). On the relationship between fapar and ndvi. *Remote Sensing of Environment*, 49(3), 200–211.
- Richter, R. & Schläpfer, D. (2014). Atmospheric/topographic correction for airborne imagery: atcor-4 user guide, version 6.3.2. DLR IB, 565–02.
- Richter, R. & Schläpfer, D. (2002). Geo-atmospheric processing of airborne imaging spectrometry data. part 2: atmospheric/topographic correction. *International Journal of Remote Sensing*, 23(13), 2631–2649.
- Ritter, N., Ruth, M., Grissom, B. B., Galang, G., Haller, J., Stephenson, G., ..., Stickley, J., et al. (2000). Geotiff format specification geotiff revision 1.0. URL: <http://www.remotesensing.org/geotiff/spec/geotiffome.html>.
- Sellers, P. J. (1985). Canopy reflectance, photosynthesis and transpiration. *International Journal of Remote Sensing*, 6(8), 1335–1372.
- Sellers, P., Dickinson, R., Randall, D., Betts, A., Hall, F., Berry, J., ..., Nobre, C., et al. (1997). Modeling the exchanges of energy, water, and carbon between continents and the atmosphere. *Science*, 275(5299), 502–509.



<i>Title:</i> NEON Algorithm Theoretical Basis Document (ATBD): Fraction of Photosynthetically Active Radiation		<i>Date:</i> 03/28/2022
<i>NEON Doc. #:</i> NEON.DOC.003840	<i>Author:</i> T. Goulden	<i>Revision:</i> B

Sellers, P., Randall, D., Collatz, G., Berry, J., Field, C., Dazlich, D., ... Bounoua, L. (1996). A revised land surface parameterization (sib2) for atmospheric gcms. part i: model formulation. *Journal of climate*, 9(4), 676–705.

Tucker, C. J. (1979). Red and photographic infrared linear combinations for monitoring vegetation. *Remote sensing of Environment*, 8(2), 127–150.

Wang, Y., Woodcock, C. E., Buermann, W., Stenberg, P., Voipio, P., Smolander, H., ..., Knyazikhin, Y., et al. (2004). Evaluation of the modis lai algorithm at a coniferous forest site in finland. *Remote sensing of Environment*, 91(1), 114–127.

Wolf, P. & Ghilani, C. (2006). *Adjustment computations spatial data analysis*. Hoboken.